Seasonal photoacclimation in the North Pacific Transition Zone

Gregory L. Britten[1,†], Christine Padalino[1,2†], Gaël Forget[1], Michael J. Follows[1]

[1]Program in Atmospheres, Oceans, and Climate, Massachusetts Institute of Technology

[2]Department of Chemical Engineering, Massachusetts Institute of Technology

Corresponding author: Gregory L. Britten (gbritten@mit.edu)

†Both authors contributed equally

Key Points:

- Seasonal variations in North Pacific chlorophyll show a distinct latitudinal structure in phase and magnitude
- Chlorophyll concentrations are negatively correlated with carbon concentrations in the transition zone (30-40°N)
- Latitudinally varying nutrient and light supply drive chlorophyll and carbon covariation via photoacclimation

Abstract

The Transition Zone Chlorophyll Front (TZCF) is a dynamic region of elevated chlorophyll concentrations in the Northeast Pacific that migrates from a southern winter (February) extent of approximately 30°N to a northern summer (August) extent of approximately 40°N. The transition zone has been highlighted as important habitat for marine animals and fisheries. We re-examine the physical and biological drivers of seasonal TZCF variability using a variety of remote sensing, reanalysis, and *in-situ* datasets. Satellite-based remote sensing estimates of chlorophyll and carbon concentrations show that seasonal TZCF migration primarily reflects a seasonal increase in the chlorophyll to carbon ratio, rather than changes in phytoplankton carbon. We use our data compilation to demonstrate how the seasonality of light and nutrient fluxes decouple chlorophyll and carbon seasonality at the transition zone latitudes. Seasonal mixed-layer-averaged light availability is positively correlated with carbon and negatively correlated with chlorophyll through the transition zone, while climatological nitrate profiles show that chlorophyll to carbon ratios are facilitated by wintertime nitrate entrainment. These empirical results are consistent with physiological data and models describing elevated chlorophyll to carbon ratios in low light, nutrient-replete environments, demonstrating the importance of latitudinal structure in interpreting seasonal chlorophyll dynamics at the basin scale.

Plain Language Summary

Satellite-observed marine chlorophyll concentrations are regularly interpreted as phytoplankton carbon. However, the chlorophyll content of cells can vary due to several environmental factors, thus complicating the interpretation of satellite-observed chlorophyll variability. In this study, we examine the relationship between chlorophyll and phytoplankton carbon in the Northeast Pacific – a region that has been highlighted as important habitat for marine animals. We find that satellite-observed chlorophyll seasonality is strongly correlated with light and nutrient availability but relatively uncorrelated with phytoplankton carbon due to changes in the chlorophyll to carbon ratio. Deep winter mixed layers are the primary physical factor driving the seasonal cycle in light and nutrient availability. These results provide a new perspective on marine ecosystem productivity in the Northeast Pacific and demonstrate how latitudinal differences in the seasonality of light and nutrient fluxes connect chlorophyll and carbon dynamics at the basin scale.

1 Introduction

The North Pacific Transition Zone Chlorophyll Front (TZCF) is a basin-scale chlorophyll feature noted in early satellite observations of ocean colour (Glover et al., 1994). The front exhibits marked seasonality, moving from a summertime northern position at approximately 40°N, to a wintertime southern position at approximately 30°N (Figure 1; Follett et al., 2021). The transition zone (30-40°N) has been repeatedly highlighted as a congregation area for marine animals and fisheries (Block et al., 2011; Hazen et al., 2013; Kappes et al., 2010; Polovina et al., 2017; Xu et al., 2017). Tagging data, where animals are fitted with geo-locators, have shown migratory and feeding behaviors throughout the transition zone, including commercially

important tuna (Polovina et al., 2017; Xu et al., 2017), seabirds (Block et al., 2011; Kappes et al., 2010), and a variety of other marine animals (Block et al., 2011; Hazen et al., 2013).

Since early satellite observations, several studies have investigated the physical, chemical, and biological drivers of TZCF variability, with authors noting the uniqueness of the apparent wintertime productivity maximum at mid-latitudes (Ayers & Lozier, 2010; Bograd et al., 2004; Chai et al., 2003; Glover et al., 1994; Le et al., 2019; Polovina et al., 2001, 2017). Glover & Mcclain (1994) and Chai et al. (2003) suggested that deep winter mixed layers entrain nitrate and drive the apparent wintertime productivity maximum, while Ayers & Lozier (2010) and Le et al. (2019) suggested a stronger role for southward Ekman transport of nitrate.

Implicit in these earlier studies of TZCF dynamics is the assumption that the observed chlorophyll variability corresponds to changes in phytoplankton carbon, while not considering potential seasonal variations in chlorophyll to carbon ratios. Like other mid- and high-latitude environments, the transition zone is characterized by large seasonal cycles in surface irradiance and mixed layer depth which drives low wintertime light availability and elevated nutrient fluxes to the mixed layer. The seasonal mixed layer cycle acts reduces light supply due to the exponential extinction of light with depth while entraining nutrients if deep mixed layer penetrate a strongly sloping nutricline (Evans et al., 1985). Physiological data and models show that nutrient-replete, low light environments will increase the ratio of chlorophyll to carbon via photoacclimation (Behrenfeld et al., 2016; Geider et al., 1996, 1998; Inomura et al., 2020; Laws & Bannister, 1980; Westberry et al., 2008).

Behrenfeld et al., (2005) and others (e.g. Graff et al., 2016) leveraged correlations between satellite-observed backscatter and phytoplankton carbon to demonstrate physiologically interpretable decoupling of phytoplankton carbon and chlorophyll in response to light and nutrient availability. From these relationships, we expect the North Pacific TZCF chlorophyll signal to, in part, reflect photoacclimation responses to seasonal variations in light and nutrient availability rather than variations in the underlying phytoplankton carbon. We test this expectation by studying the latitudinal structure of surface chlorophyll and carbon variations using a variety of remote sensing, reanalysis, and *in-situ* datasets. We disentangle the role of photoacclimation in the observed TZCF chlorophyll dynamics by quantifying relationships between chlorophyll concentrations, carbon concentrations, net primary productivity, light availability, and mixed layer depths over the seasonal cycle. We examine these relationships across latitudes to identify the unique chlorophyll cycle in the transition zone. These results will help better understand ecosystem productivity in the North Pacific and improve our interpretation of the mid-latitude satellite chlorophyll record.

2 Methods

We assembled a variety of remote sensing, reanalysis, and *in-situ* datasets to examine the latitudinal structure of chlorophyll and carbon variations and the dynamics of photoacclimation at the TZCF. Satellite remote sensing estimates of surface chlorophyll concentrations, carbon concentrations, net primary productivity, surface photosynthetically active radiation (PAR), and the diffuse attenuation coefficient (k_d) were obtained from the Oregon State Ocean Productivity database (http://sites.science.oregonstate.edu/ocean.productivity/). These estimates have been gap-filled for missing observations due to cloud cover according to the algorithm described at http://orca.science.oregonstate.edu/gap_fill.php. Chlorophyll concentrations are based on the

Generalized Inherent Optical Property Algorithm (GIOP) using MODIS observations (Werdell et al., 2013). Carbon concentrations are based on backscatter coefficients estimated via the GIOP algorithm, modeled via the functions given in Behrenfeld et al., (2005) and Westberry et al., (2008). We also repeated analyses using chlorophyll and carbon concentrations derived from the alternative Garver-Siegel-Maritorena (GSM) ocean color inversion algorithm (Maritorena et al., 2002) to ensure the consistently of results across inversion products. Net primary productivity was taken from four models that differ in their parameterization of phytoplankton growth: the vertically generalized productivity model (VGPM; Behrenfeld & Falkowski, 1997), the carbon-based productivity model (CBPM; Westberry et al., 2008), the Eppley vertically generalized productivity model (EPVGPM; http://sites.science.oregonstate.edu/ocean.productivity/eppley.model.php), and the Carbon, Absorption, and Fluorescence Euphotic-resolving model (CAFÉ; Silsbe et al., 2016). Surface PAR and k_d are estimated from MODIS observations (Son & Wang, 2015).

Reanalysis datasets of mixed layer depth were obtained from the simple ocean data assimilation product (SODA; version SODA3 12.2; available at https://www.soda.umd.edu/) and the Hybrid Coordinate Ocean Model (HyCOM; hindcast version GLBu0.08; available at http://sites.science.oregonstate.edu/ocean.productivity). SODA mixed layers were linearly interpolated from the original five-day interval to an eight-day interval to match the satellite and HyCOM datasets obtained from the Oregon State Productivity Database. We obtained mixed layer estimates from Argo based on the methods of Holte et al., (2017) (http://mixedlayer.ucsd.edu/). In the supplementary material we demonstrate a high correlation between SODA, HyCOM, and Argo mixed layer estimates (**Supplementary Figure S1**), indicating robustness across mixed layer depth products. All satellite and reanalysis datasets were bilinearly interpolated onto a common 0.5º grid. Climatological nitrate observations were taken from the World Ocean Atlas, version WOA2018 (Garcia et al., 2019). Mixed layer-averaged irradiance was calculated according to

$$\bar{I} = \frac{1}{z_{ml}} \int_{z_{ml}}^{0} I(z)dz = \frac{1}{k_d z_{ml}} I_0 e^{-k_d z_{ml}} (1 - e^{-k_d z_{ml}}),$$

where $I(z)$ is the scaler irradiance at depth z, k_d is the diffuse attenuation coefficient, z_{ml} is the depth of the mixed layer, and I_0 is the PAR incident at the sea surface. Entrainment nitrate fluxes into the mixed layer during mixed layer deepening were calculated according to

$$F_N = \frac{dz_{ml}}{dt} (N_0 - N_{ml}),$$

where $\frac{dz_{ml}}{dt}$ is the entrainment velocity, N_0 is the nitrate concentration one meter below the mixed layer according a linear interpolation of World Ocean Atlas nitrate profiles, and N_{ml} is the mixed layer-averaged nitrate concentration.

To investigate the latitudinal structure of chlorophyll and carbon dynamics, we binned observations according to six latitude bands across the Northeast Pacific, defined by longitudinal bounds of -180ºW to -115ºW. Latitudinal bands were defined by the intervals 0-10ºN, 10-20ºN, 20-30ºN, 30-40ºN, 40-50ºN, 50-60ºN. The western bound of -180ºW was adopted to avoid influence of the western boundary current which imparts stochastic variability on the physical and chemical properties compared to the more stable latitudinal structure observed in the central and eastern reaches of the basin.

3 Results

3.1 Covariation between chlorophyll and carbon

The seasonal TZCF migration is readily observed by comparing chlorophyll maps for the months of August and February (**Figure 1a,d**). August corresponds to the month of the maximum northward extent at approximately 40ºN, while February corresponds to the month of maximum southward extent at approximately 30ºN. Transition zone chlorophyll concentrations are elevated three- to five-fold during the February chlorophyll maximum, relative to August. While February is the month of maximum transition zone chlorophyll, concentrations are elevated over the months of January-February-March which we hereafter refer to as transition zone winter.

Climatological maps demonstrate that February transition zone chlorophyll does not spatially correlate to carbon concentrations across the basin (**Figure 1**). The transition zone shows no appreciable increase in February carbon concentrations relative to August. February carbon concentrations are also depressed to the north and south of the transition zone, in contrast to chlorophyll which remains elevated to the north. The seasonal decoupling between chlorophyll and carbon becomes clear in the climatological distribution of the chlorophyll to carbon ratio (**Figure 1c,f**), where ratios are elevated roughly five-fold in winter from the transition zone northward. Primary productivity models also disagree on the magnitude and spatial pattern of wintertime transition zone productivity with no consistent spatial correlation with chlorophyll (**Supplementary Figure S2**). Notably, the two productivity models that include photoacclimation processes (CBPM and CAFÉ) estimate productivity south of the transition zone to be more than double that of productivity models that do not include photoacclimation (VGPM and Epply VGPM), again reflecting the decoupling of chlorophyll and carbon, here with consequences for satellite-based productivity estimates.

The temporal dynamics of chlorophyll and carbon concentration time series clearly demonstrate the latitudinal dependence of covariation between the two variables (**Figure 2**). Over the seasonal cycle, chlorophyll concentrations in the transition zone are negatively correlated with carbon concentrations (r=-0.40, **Figure 2c**). Negative correlations between chlorophyll and carbon extend from 10-40°N, with the strongest negative correlation at 20-30°N (r=-0.77; **Figure 2d**). However, mean transition zone chlorophyll concentrations are several-fold higher than more southern latitudes with a seasonal chlorophyll range of approximately 0.2 mgChl/m^3, highlighting the strength of the TZCF signal. Across latitudes, the seasonal correlation between chlorophyll and productivity is also negative in the transition zone when averaging over four primary productivity models (r=-0.11), with positive correlations between chlorophyll and productivity at more northern and southern latitudes (**Supplementary Figure S3)**. Across years, negative correlations between chlorophyll and carbon are driven by a consistent offset in the timing of their respective seasonal maxima, reflecting the chlorophyll peak in photoacclimated low light conditions (**Figure 3**). All latitudes show an average lag between chlorophyll and carbon maxima, with chlorophyll consistently peaking prior to carbon. The average lag across latitudes is 90 days with a standard deviation of 95 days. The most consistent lag was found in the transition zone, with a mean offset of 93 days and a standard deviation of 25 days across years (**Figure 3**). Taken together, the negative correlations between transition zone chlorophyll and carbon concentrations demonstrate the unique latitudinal structure of the chlorophyll cycle

across the North Pacific. The transition zone exhibits a high-amplitude chlorophyll cycle that is largely independent of variations in phytoplankton carbon.

3.2 Relationships with mixed layer depth and light availability

The seasonal covariation of chlorophyll and carbon across latitude can be interpreted in terms of latitude-specific responses to seasonal mixed layer depth variability and the resulting impact on nutrient and light availability (**Figure 4**). Across latitudes, we find a consistently negative relationship between mixed layer depth and carbon, with the strength of the relationship decreasing southward (**Figure 4a-f**). In contrast, we find both positive and negative correlations between mixed layer depth and chlorophyll across latitudes, with the largest positive slope in the transition zone (**Figure 4i**). The consistent positive slope of the transition zone chlorophyll relationship combines with a large range of seasonal mixed layer depths (20-145m) to a yield a transition zone chlorophyll cycle that is well predicted from a linear relationship with mixed layer depth.

The correlation of mixed layer and light availability is shown in **Figure 5**. Large seasonal cycles in surface irradiance and mixed layer depth are apparent at mid- and high-latitudes (**Figure 5a-b**). The mean surface irradiance (around which the seasonal cycle oscillates) decreases northward, with the summer maximum surface irradiance at 50-60°N roughly equal to wintertime light availability in the tropics. Combining surface irradiance, mixed layer depth, and satellite estimates of the light attenuation coefficient k_d, we find that the largest seasonal cycle in mixed layer-averaged irradiance occurs in the transition zone, with a climatological seasonal amplitude of approximately 170μMol quanta/m^2/s and a wintertime light availability less than 10μMol quanta/m^2/s (**Figure 5c**). The minimal light availability in the transition zone winter thus approaches the minimum compensation irradiance of photosynthesis (Geider et al., 1986; Venables & Moore, 2010), highlighting the severe light limitation experienced by the wintertime transition zone phytoplankton community.

The distinct responses of transition zone carbon and chlorophyll to mixed layer depth and light availability are shown spatially by mapping the seasonal correlation coefficients across the basin (**Figure 6**). The correlation of mixed layer depth vs. carbon concentration is negative across most of the basin, with a band of weaker correlations in the transition zone (**Figure 6a**). Conversely, correlations of mixed layer depth vs. chlorophyll are weak across much of the basin, except for the band of strong negative correlations across the transition zone (**Figure 6b**). These patterns further demonstrate that deepening winter mixed layers drive increases in chlorophyll concentrations in the transition zone that are uncorrelated with variations in carbon. In terms of mixed layer-averaged irradiance, we see weak positive correlations with carbon north of 20°N ($r \sim 0.20$) and weak negative correlations southward ($r \sim -0.10$; **Figure 6c**). In contrast to carbon and consistent with photoacclimation, chlorophyll strongly correlates with mixed layer-averaged irradiance throughout the transition zone, with correlations between -0.5 and -0.7 (**Figure 6d**). Zonally-averaged correlations reiterate this picture, showing diverging responses of carbon and chlorophyll with respect to mixed layer depth and mixed layer-averaged irradiance in the transition zone (**Figure 7**). We note that the correlation analysis was repeated using the alternative mixed layer reanalysis from SODA (**Supplementary Figures S4 and S5**). We found

no appreciable difference in the magnitudes or spatial structure of the calculated correlations, indicating robustness in these relationships across mixed layer depth estimates.

Re-expressing relationships between light, carbon, and chlorophyll in terms of the chlorophyll to carbon ratio (Chl:C) reveals a strong nonlinear association between Chl:C and mixed layer-averaged irradiance, driven by nonlinear increases in Chl:C at the lowest light availability (**Figure 8**). The relationship between Chl:C and mixed layer-averaged irradiance is well-described by a negative exponential with light supply, like those described previously based on physiological principles (Behrenfeld et al., 2005; Graff et al., 2016; Jackson et al., 2017; Sathyendranath et al., 2020). The nonlinear response of Chl:C occurs in the light-limited regime encountered during transition zone winter.

3.2 Mixed layer driven nutrient availability

Deepening mixed layers can also act to entrain nutrients as deepening mixed layers penetrate layers of elevated nutrient concentrations. The resulting nutrient supply can then further enhance chlorophyll to carbon ratios due to the nitrogen requirement of chlorophyll and light harvesting protein synthesis, as faster growth rates require more chlorophyll for a given light level (Geider et al., 1998; Inomura et al., 2020). The entrainment nitrate flux is composed of the entrainment velocity from deepening mixed layers $\frac{dz_{ml}}{dt}$ and the nitrate gradient at the base of the mixed layer. We find significant seasonality in entrainment velocity from 20°N and northward, with a maximum velocity that increases with latitude (**Figure 9a-b**). Similar latitudinal patterns are found in the mean nitrate gradient at the base of the mixed layer, with the mean gradient increasing northward beyond the equatorial latitudes (**Figure 9c**). The seasonal cycle in the subsurface nitrate gradient shows a more distinct latitudinal pattern. Nitrate uptake in the spring and summer drives the gradient from 20-40°N near zero in summer. This pattern contrasts with latitudes to the north and south of 20-40°N where spring and summer nitrate depletion is less severe. The entrainment velocity and nitrate gradient combine to yield a seasonal cycle of entrainment nitrate flux with an amplitude that increases with latitude (**Figure 9d**). Wintertime nitrate flux exceeds 30 mmol/m^2/month north of 40°N and exceeds 10 mmol/m^2/month in the transition zone, while remaining several fold lower southward. These results demonstrate that the transition zone latitudes of 30-40°N is the most southern latitude to receive a significant wintertime nitrate entrainment flux, consistent with arguments of Glover et al., (1994).

To ensure robustness of our results, we repeated all chlorophyll and carbon analyses above using estimates from the alternative GSM ocean colour inversion algorithm (Maritorena et al., 2002). Although low latitude GSM chlorophyll concentration magnitudes were slightly higher than GIOP estimates and low latitudes carbon slightly higher, the seasonality in the two inversions was highly consistent, reproducing the correlations reported above. All results using GSM estimates are reported in the Supplemental Information (Figures S6-10).

4 Discussion

4.1 Photoacclimation as a primary driver of wintertime transition zone chlorophyll

The observed negative covariation of chlorophyll and carbon in the transition zone, and its relationships with light and nutrient availability, demonstrate photoacclimation as a primary

driver of chlorophyll variability in the TZCF. Consistent with earlier satellite-based (Behrenfeld et al., 2005) and physiological (Behrenfeld et al., 2016; Geider et al., 1996, 1998; Inomura et al., 2020; Laws & Bannister, 1980; Talmy et al., 2013) analyses, the wintertime increase in transition zone chlorophyll appears to be due to an increase in the chlorophyll to carbon ratio in response to light-limited, nutrient-replete growth conditions. Extending this earlier work, we explicitly resolve the latitudinal structure of photoacclimation dynamics at the basin scale and link the decoupling of chlorophyll and carbon seasonality to the observed seasonality of latitudinal light and nutrient supply.

This interpretation of TZCF chlorophyll dynamics extends previous studies investigating transition zone seasonality (Ayers & Lozier, 2010; Bograd et al., 2004; Chai et al., 2003; Glover et al., 1994; Le et al., 2019). These studies interpreted the southern extent of the wintertime chlorophyll front as a phytoplankton carbon signal and sought the necessary environmental drivers to explain elevated wintertime productivity. Our results, while supporting the existence of a significant vertical wintertime nitrate flux (Chai et al., 2003; Glover et al., 1994), suggest that wintertime nutrient supply has a limited impact on phytoplankton carbon and productivity. Instead, wintertime nitrate supply relaxes nutrient stress, thus enriching the growth environment to provide nutrients to fully acclimatize to light-limited conditions. Laboratory observations show that nutrient stress decreases the chlorophyll to carbon ratio in light-lighted conditions by diverting nitrogen from pigments and light-harvesting proteins (Geider et al., 1996; Inomura et al., 2020; Laws & Bannister, 1980), supporting the suggestion that wintertime nutrient supplies help maximize the seasonal photoacclimation response at transition zone latitudes. Established empirical models also show a positive relationship between surface nitrate concentrations and the N:C of particulate biomass (Galbraith & Martiny, 2015) which further suggest that phytoplankton are able to build nitrogen rich pigments and light-harvesting proteins at high nitrate supply.

This new perspective on seasonal chlorophyll dynamics in in the transition zone may motivate re-analysis of higher trophic animal usage patterns in the region. Niche models for marine mammals and seabirds have used satellite chlorophyll to represent bottom up drivers (Abrahms et al., 2018; Block et al., 2011; Hazen et al., 2013). However, our results suggest that chlorophyll serves as a poor proxy for transition zone phytoplankton carbon and that high chlorophyll levels indicate a relatively low carbon content of cells, either though seasonal succession of low-light adapted species or intra-specific acclimation. Because chlorophyll correlates strongly with sea surface temperature (Bograd et al., 2004), periods of decorrelation between chlorophyll and phytoplankton carbon, as characterized here, may provide the opportunity to isolate the roles of temperature and food availability on animal habitat utilization.

4.2 General implications for satellite observing of marine ecosystems

This study reiterates the need to account for photoacclimation when interpreting the satellite chlorophyll record, echoing calls from previous authors (Behrenfeld et al., 2005, 2016; Fox et al., 2020; Graff et al., 2016; Omta et al., 2009). Although the dynamics and interannual trends in chlorophyll have been insightful (Ayers & Lozier, 2010; Boyce et al., 2010, 2017; Glover et al., 1994; Hammond et al., 2020), many studies continue to use chlorophyll as a proxy for phytoplankton carbon and productivity. Complex relationships between chlorophyll, carbon, and

productivity, including the latitudinal dependence demonstrated here, complicate this interpretation.

Beyond the North Pacific, our results suggest further work to elucidate the latitudinal structure of light and nutrient supplies globally to better understand their role in coupling chlorophyll and carbon dynamics. In the North Pacific, winter conditions conspire at the 30-40°N band to exhibit deep winter mixing that drives a large seasonal cycle in light and nutrient supply which maximizes seasonal photoacclimation; however, it is not clear whether the seasonal cycles of light and nutrient supply in other basins will show similar latitudinal structure.

The relationship between mixed layer-averaged irradiance and Chl:C also has important implications for observing climate impacts on marine ecosystems (Behrenfeld et al., 2016), including multiple studies that have examined multidecadal trends in chlorophyll (Boyce et al., 2010; Hammond et al., 2020; Henson et al., 2010). Warming of the upper water column has increased stratification and reduced mixed layer depths in the North Pacific (Freeland, 2013) and across the global ocean (Li et al., 2018), with trends expected to increase into the future (Fu et al., 2016). These changes are often associated with reduced nutrient supply and productivity (Behrenfeld et al., 2006; Fu et al., 2016), which are invoked to explain chlorophyll declines. However, photoacclimation dynamics suggest that chlorophyll declines may also occur with reduced mixed layers due to photoacclimation (higher light availability with mixed layer shoaling) and may be uncorrelated or negatively correlated with changes in phytoplankton carbon and productivity (Behrenfeld et al., 2016).

Going forward, we highlight the need to further integrate eco-physiology with satellite observing of marine ecosystems to better understand the physiological growth conditions of phytoplankton at large spatial scales. Continued progress has been made with carbon-based estimates of ocean productivity that explicitly account for photoacclimation processes (Behrenfeld et al., 2005, 2016; Fox et al., 2020; Westberry et al., 2008). More recent work has further integrated resource-allocation strategies into remote sensing models of phytoplankton growth (Tanioka et al., 2020) which provide additional constraints on phytoplankton physiology by resolving cellular stoichiometry as a function of light, nutrient supply, and temperature (Geider et al., 1998; Inomura et al., 2020; Laws & Bannister, 1980).

5 Conclusions

In conclusion, our results suggest chlorophyll variability in the transition zone is primarily driven by photoacclimation to nutrient replete, light-limited growth conditions found in the transition zone winter. The latitudinal structure of seasonal light and nutrient supply creates conditions that maximize seasonal photoacclimation and govern the TZCF chlorophyll signal. Further synthesis of phytoplankton physiology and carbon-based remote-sensing of marine ecosystems will improve our understanding of the phytoplankton growth environment and reduce uncertainties in detecting climate change impacts on ocean ecosystems from space.

Acknowledgments

We acknowledge all the observational scientists and technologists that made this work possible. GLB acknowledges funding from the Simons Foundations Postdoctoral Fellowship in Marine Microbial Ecology. GLB, CP, GF, MJF acknowledge funding from the Simons Foundation

Collaboration on Computational Biogeochemical Modeling of Marine Ecosystems (CBIOMES) and Simons Collaboration on Ocean Processes and Ecology (SCOPE). CP acknowledges funding from the Undergraduate Research Opportunities Program at MIT. Data used in this study are available publicly through http://sites.science.oregonstate.edu/ocean.productivity/, https://www.soda.umd.edu, http://mixedlayer.ucsd.edu/ and through the World Ocean Atlas (Garcia et al., 2019). Details are given in the main text. All code to reproduce the analyses are available publicly at https://github.com/gregbritten/transition_zone_chlorophyll

References

Abrahms, B., Hazen, E. L., Bograd, S. J., Brashares, J. S., Robinson, P. W., Scales, K. L., et al. (2018). Climate mediates the success of migration strategies in a marine predator. *Ecology Letters*, *21*(1), 63–71.

Ayers, J. M., & Lozier, M. S. (2010). Physical controls on the seasonal migration of the North Pacific transition zone chlorophyll front. *Journal of Geophysical Research: Oceans*, *115*, 1–11.

Behrenfeld, M. J., & Falkowski, P. G. (1997). Photosynthetic rates derived from satellite-based chlorophyll concentration. *Limnology and Oceanography*, *42*(1), 1–20.

Behrenfeld, M. J., Boss, E., Siegel, D. A., & Shea, D. M. (2005). Carbon-based ocean productivity and phytoplankton physiology from space. *Global Biogeochemical Cycles*, *19*(1), 1–14.

Behrenfeld, M. J., O'Malley, R. T., Siegel, D. a, McClain, C. R., Sarmiento, J. L., Feldman, G. C., et al. (2006). Climate-driven trends in contemporary ocean productivity. *Nature*, *444*(7120), 752–725.

Behrenfeld, M. J., O'Malley, R. T., Boss, E. S., Westberry, T. K., Graff, J. R., Halsey, K. H., et al. (2016). Revaluating ocean warming impacts on global phytoplankton. *Nature Climate Change*, *6*(3), 323–330.

Block, B. A., Jonsen, I. D., Jorgensen, S. J., Winship, A. J., Shaffer, S. A., Bograd, S. J., et al. (2011). Tracking apex marine predator movements in a dynamic ocean. *Nature*, *475*(7354), 86–90.

Bograd, S. J., Foley, D. G., Schwing, F. B., Wilson, C., Laurs, R. M., Polovina, J. J., et al. (2004). On the seasonal and interannual migrations of the transition zone chlorophyll front. *Geophysical Research Letters*, *31*(17), 1–5.

Boyce, D. G., Lewis, M. R., & Worm, B. (2010). Global phytoplankton decline over the past century. *Nature*, *466*(7306), 591–6.

Boyce, D. G., Petrie, B., Frank, K. T., Worm, B., & Leggett, W. C. (2017). Environmental structuring of marine plankton phenology. *Nature Ecology and Evolution*, *1*(10), 1484–1494.

Chai, F., Jiang, M., Barber, R. T., Dugdale, R. C., & Chao, Y. (2003). Interdecadal variation of the Transition Zone Chlorophyll Front: A physical-biological model simulation between 1960 and 1990. *Journal of Oceanography*, *59*(4), 461–475.

Evans, G. T., Parslow, J. S., Evans, G. T., & Parslow, J. S. (1985). A model of annual plankton cycles. *Deep Sea Research Part B. Oceanographic Literature Review*, *32*(9), 759.

Follett, C. L., Dutkiewicz, S., Forget, G., Cael, B. B., & Follows, M. J. (2021). Moving ecological and biogeochemical transitions across the North Pacific. *Limnology and Oceanography*, *66*(6), 2442–2454.

Fox, J., Behrenfeld, M. J., Haëntjens, N., Chase, A., Kramer, S. J., Boss, E., et al. (2020). Phytoplankton growth and productivity in the Western North Atlantic: Observations of regional variability from the NAAMES field campaigns. *Frontiers in Marine Science*, *7*(24), 1–15.

Freeland, H. J. (2013). Evidence of change in the winter mixed layer in the Northeast Pacific Ocean: A problem revisited. *Atmosphere-Ocean*, *51*, 126–133.

Fu, W., Randerson, J. T., & Moore, J. K. (2016). Climate change impacts on net primary production (NPP) and export production (EP) regulated by increasing stratification and phytoplankton community structure in the CMIP5 models. *Biogeosciences*, *13*, 5151–5170.

Galbraith, E. D., & Martiny, A. C. (2015). A simple nutrient-dependence mechanism for predicting the stoichiometry of marine ecosystems. *Proceedings of the National Academy of Sciences*, *112*(27), 8199–8204.

Garcia, H. E., Boyer, T. P., Baranova, O. K., Locarnini, R. A., Mishonov, A. V., Grodsky, A., et al. (2019). World Ocean Atlas 2018. *Product Documentation*, *1*, 1–20.

Geider, R. J., Osborne, B. A., & Raven, J. A. (1986). Growth, photosynthesis, and maintenance metabolic cost in the diatom Phaeodactylum tricornutum at very low light levels. *Journal of Phycology*, *22*, 39–48.

Geider, R. J., MacIntyre, H. L., & Kana, T. M. (1996). A dynamic model of photoadaptation in phytoplankton. *Limnology and Oceanography*, *41*(1), 1–15.

Geider, R. J., MacIntyre, H. L., & Kana, T. M. (1998). A dynamic regulatory model of phytoplanktonic acclimation to light, nutrients, and temperature. *Limnology and Oceanography*, *43*(4), 679–694.

Glover, M., Wroblewski, J. S., & McClain, C. R. (1994). Dynamics of the transition zone in coastal zone color scanner-sensed ocean color in the North Pacific during oceanographic spring. *Journal of Geophysical Research*, *99*, 7501–7511.

Graff, J. R., Westberry, T. K., Milligan, A. J., Brown, M. B., Dall'Olmo, G., Reifel, K. M., & Behrenfeld, M. J. (2016). Photoacclimation of natural phytoplankton communities. *Marine Ecology Progress Series*, *542*, 51–62.

Hammond, M. L., Beaulieu, C., Henson, S. A., & Sahu, S. K. (2020). Regional surface chlorophyll trends and uncertainties in the global ocean. *Scientific Reports*, *10*(1), 1–9.

Hazen, E. L., Jorgensen, S., Rykaczewski, R. R., Bograd, S. J., Foley, D. G., Jonsen, I. D., et al. (2013). Predicted habitat shifts of Pacific top predators in a changing climate. *Nature Climate Change*, *3*(3), 234–238.

Henson, S. A., Sarmiento, J. L., Dunne, J. P., Bopp, L., Lima, I., Doney, S. C., et al. (2010). Detection of anthropogenic climate change in satellite records of ocean chlorophyll and productivity. *Biogeosciences*, *7*(2), 621–640.

Holte, J., Talley, L. D., Gilson, J., & Roemmich, D. (2017). An Argo mixed layer climatology and database. *Geophysical Research Letters*, *44*(11), 5618–5626.

Inomura, K., Omta, A. W., Talmy, D., Bragg, J., Deutsch, C., & Follows, M. J. (2020). A mechanistic model of macromolecular allocation, elemental stoichiometry, and growth rate in phytoplankton. *Frontiers in Microbiology*, *11*, 1–9.

Jackson, T., Sathyendranath, S., & Platt, T. (2017). An exact solution for modeling photoacclimation of the carbon-to-chlorophyll ratio in phytoplankton. *Frontiers in Marine Science*, *4*, 1–10.

Kappes, M. A., Shaffer, S. A., Tremblay, Y., Foley, D. G., Palacios, D. M., Robinson, P. W., et al. (2010). Hawaiian albatrosses track interannual variability of marine habitats in the North Pacific. *Progress in Oceanography*, *86*(2), 246–260.

Laws, E. A., & Bannister, T. T. (1980). Nutrient- and light-limited growth of Thalassiosira fluviatilis in continuous culture with implications for phytoplankton growth in the ocean. *Limnology and Oceanography*, *25*, 457–473.

Le, C., Wu, S., Hu, C., Beck, M. W., & Yang, X. (2019). Phytoplankton decline in the eastern North Pacific transition zone associated with atmospheric blocking. *Global Change Biology*, *25*(10), 3485–3493.

Li, G., Cheng, L., Zhu, J., Trenberth, K. E., Mann, M. E., & Abraham, J. P. (2018). Increasing ocean stratification over the past half-century. *Nature Climate Change*, (12), 1116–1123.

Maritorena, S., Siegel, D. A., & Peterson, A. R. (2002). Optimization of a semianalytical ocean color model for global-scale applications. *Applied Optics*, *41*(15), 2705.

Omta, A. W., Llido, J., Garçon, V., Kooijman, S. A. L. M., & Dijkstra, H. A. (2009). The interpretation of satellite chlorophyll observations: The case of the Mozambique Channel. *Deep-Sea Research Part I: Oceanographic Research Papers*, *56*(6), 974–988.

Polovina, J. J., Howell, E., Kobayashi, D. R., & Seki, M. P. (2001). The transition zone chlorophyll front, a dynamic global feature defining migration and forage habitat for marine resources. *Progress in Oceanography*, *49*, 469–483.

Polovina, J. J., Howell, E. A., Kobayashi, D. R., & Seki, M. P. (2017). The Transition Zone Chlorophyll Front updated: Advances from a decade of research. *Progress in Oceanography*, *150*, 79–85.

Sathyendranath, S., Platt, T., Kovač, Ž., Dingle, J., Jackson, T., Brewin, R. J. W., et al. (2020). Reconciling models of primary production and photoacclimation. *Applied Optics*, *59*(10), 100–114.

Silsbe, G., Behrenfeld, M., Halsey, K., Milligan, A., & Westberry, T. (2016). The CAFE model: A net production model for global ocean phytoplankton. *Global Biogeochemical Cycles*, *30*, 1756–1777.

Son, S. H., & Wang, M. (2015). Diffuse attenuation coefficient of the photosynthetically available radiation Kd(PAR) for global open ocean and coastal waters. *Remote Sensing of Environment*, *159*, 250–258.

Talmy, D., Blackford, J., Hardman-Mountford, N. J., Dumbrell, A. J., & Geider, R. J. (2013). An optimality model of photoadaptation in contrasting aquatic light regimes. *Limnology and Oceanography*, *58*(5), 1802–1818.

Tanioka, T., Fichot, C. G., & Matsumoto, K. (2020). Toward determining the spatio-temporal variability of upper-ocean ecosystem stoichiometry from satellite remote sensing. *Frontiers in Marine Science*, *7*, 1–16.

Venables, H., & Moore, C. M. (2010). Phytoplankton and light limitation in the Southern Ocean: Learning from high-nutrient, high-chlorophyll areas. *Journal of Geophysical Research*, *115*, 1–12.

Werdell, P. J., Franz, B. A., Bailey, S. W., Feldman, G. C., Boss, E., Brando, V. E., et al. (2013). Generalized ocean color inversion model for retrieving marine inherent optical properties. *Applied Optics*, *52*, 2019–2037.

Westberry, T., Behrenfeld, M. J., Siegel, D. A., & Boss, E. (2008). Carbon-based primary productivity modeling with vertically resolved photoacclimation. *Global Biogeochemical Cycles*, *22*(2), 1–18.

Xu, Y., Nieto, K., Teo, S. L. H., McClatchie, S., & Holmes, J. (2017). Influence of fronts on the spatial distribution of albacore tuna (Thunnus alalunga) in the Northeast Pacific over the past 30 years (1982–2011). *Progress in Oceanography*, *150*, 72–78.

485

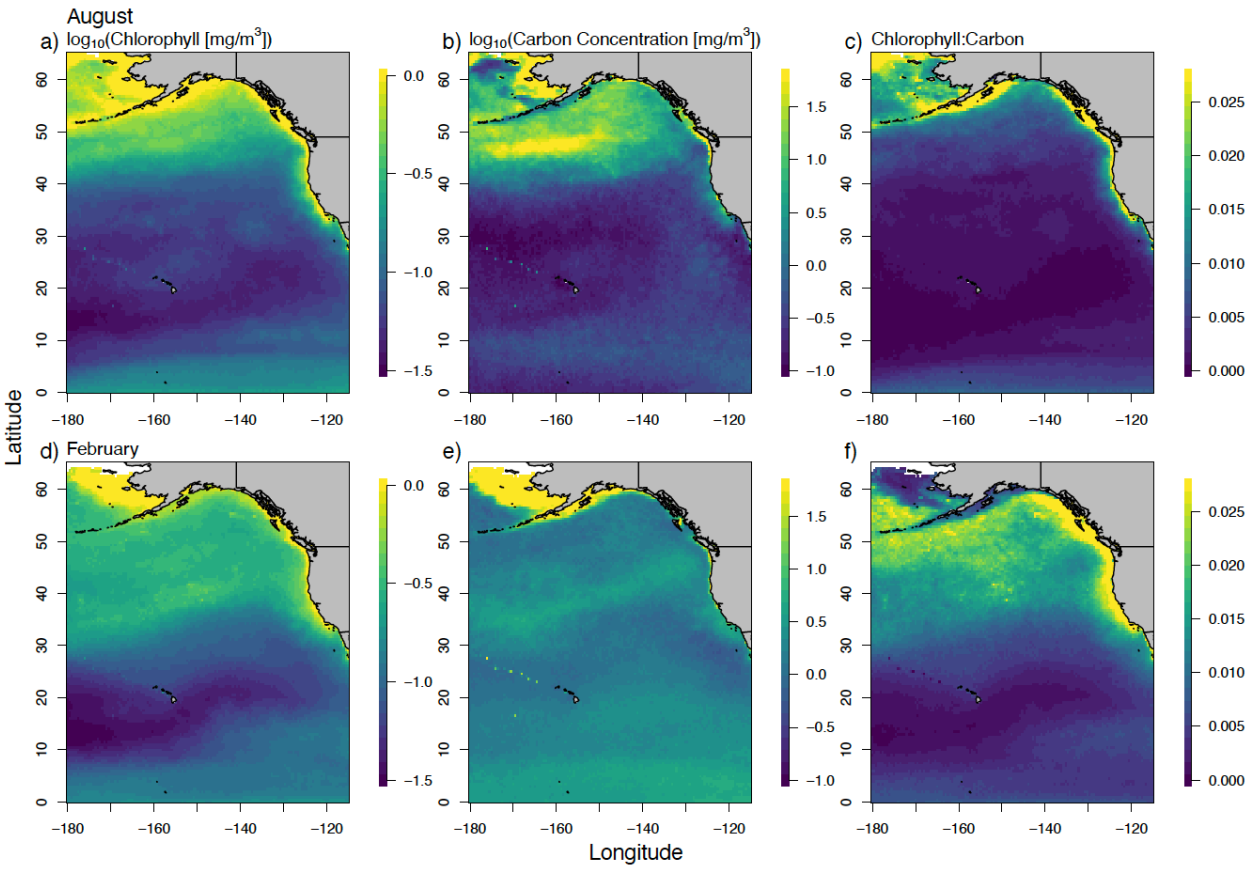

486

487 **Figure 1. Satellite-estimated climatology for surface chlorophyll concentrations, carbon**
488 **concentrations, and their ratio for the months of August and February in the Northeast**
489 **Pacific.** Panels a-c give the climatological chlorophyll, carbon, and chlorophyll:carbon ratio
490 distributions for August, respectively. Panels d-f give the same respective fields for February.
491

492

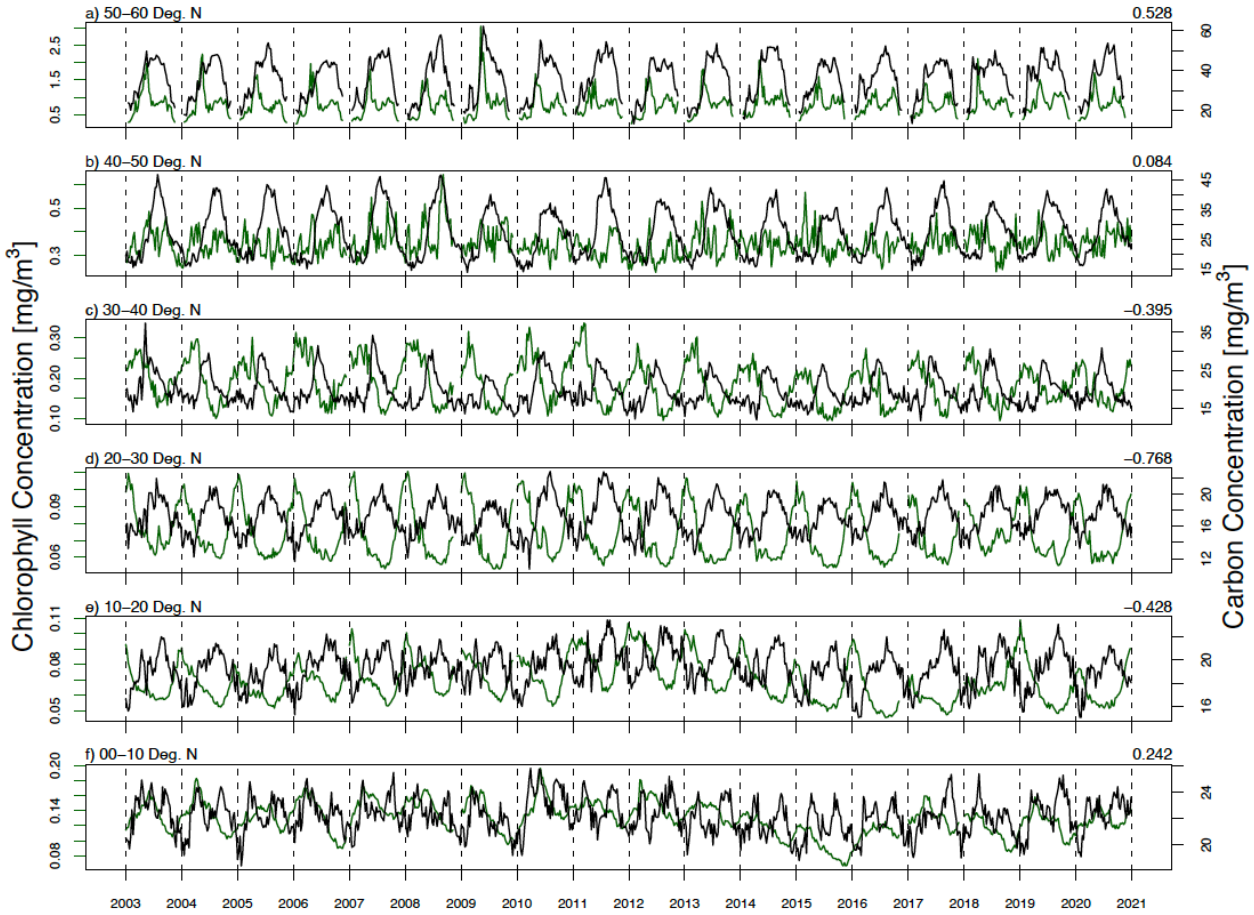

493

494 **Figure 2. Latitudinal time series of chlorophyll and carbon concentrations.** Chlorophyll is
495 given with green lines and carbon is given with black. Rows represent different latitude bands.
496 Latitudinal range is given in the top left of each panel. Correlation coefficient between the two
497 series is given in the top right of each panel. Vertical dashed lines show January 01 of each year.
498 Note the differing axis limits across panels.

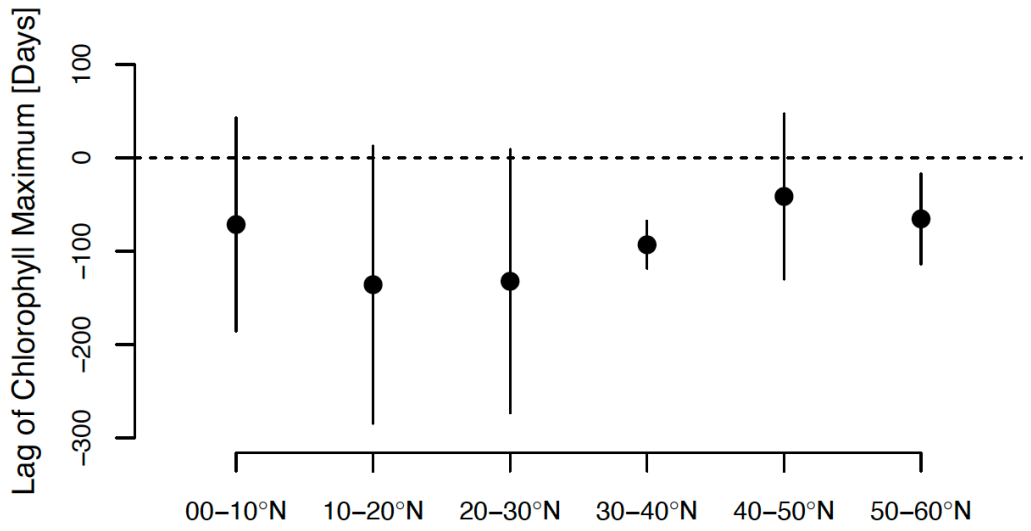

Figure 3. Means and standard deviations of the lag between seasonal chlorophyll and carbon maxima. Maxima are taken within individual years according to latitudinal time series in Figure 2. Mean and standard deviations are calculated across years. Negative values indicate that chlorophyll peaks before carbon in the seasonal cycle.

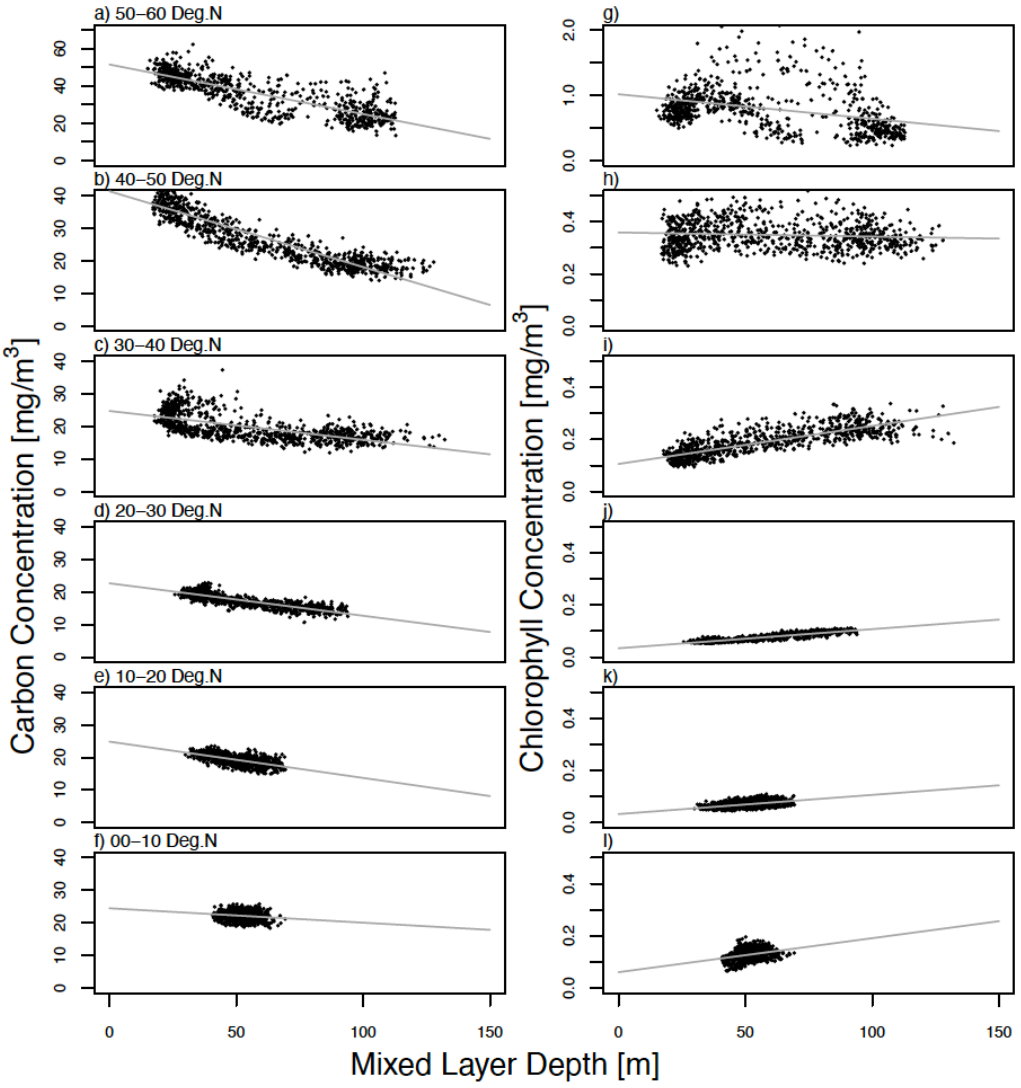

507

508 **Figure 4. Latitudinal relationships between carbon and chlorophyll concentrations with**
509 **respect to mixed layer depth.** Left column (panels a-f) gives the relationships between carbon
510 and mixed layer depth. Right column (panels g-l) gives the relationships with chlorophyll. Rows
511 are latitude bands as in Figure 2. Latitude range is given in the top left of left column panels.
512 Grey lines give the ordinary least squares regression line.

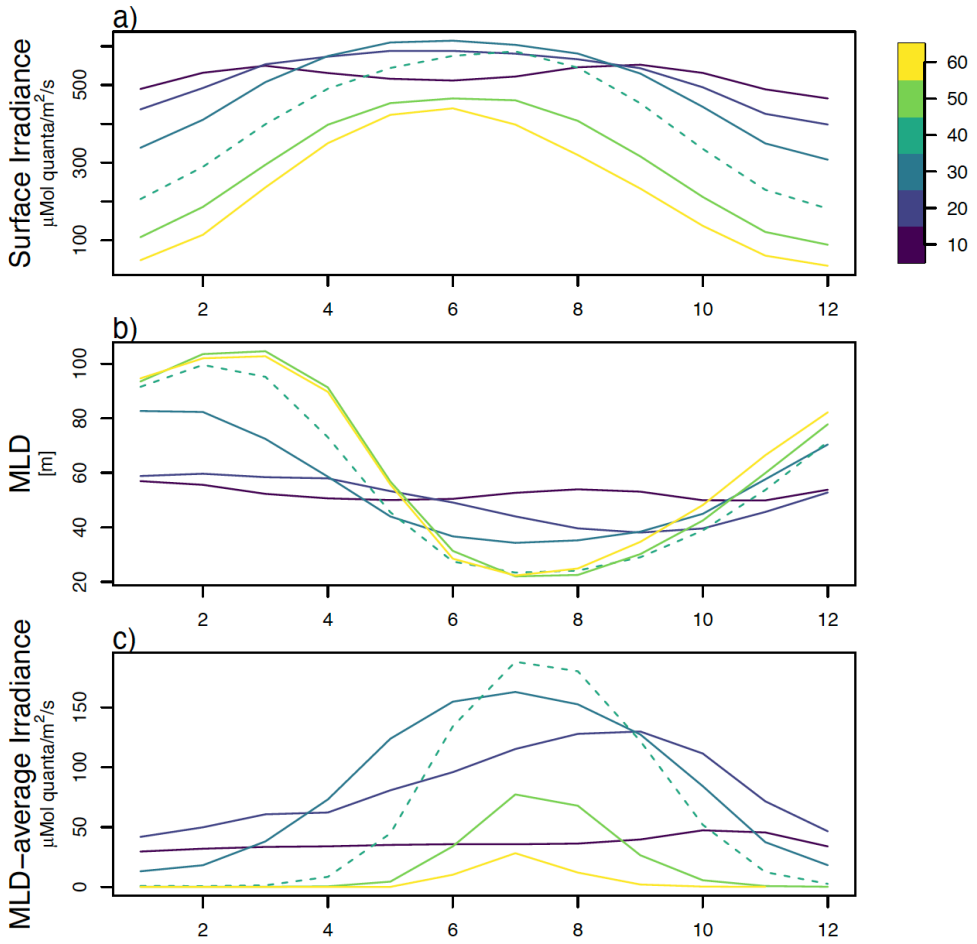

Figure 5. Seasonal climatology of day-averaged surface irradiance (a), mixed layer depth (b), and day-averaged mixed layer-averaged irradiance (c) for ten-degree latitude bands in the Northeast Pacific. Color bar gives the latitude bands for each line. Dashed line indicates the transition zone (30-40°N).

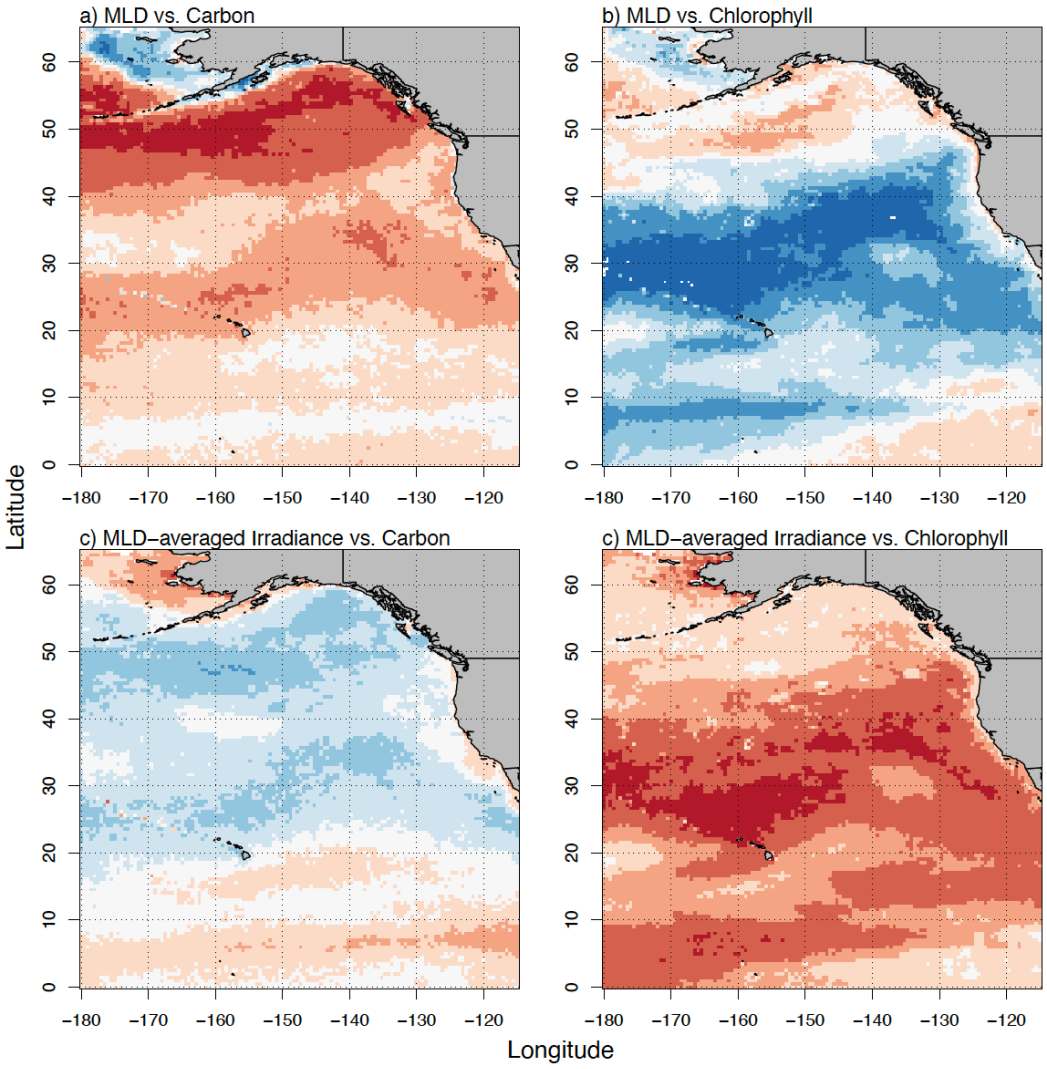

Figure 6. Time series correlation coefficients between mixed layer depth (MLD) vs. carbon concentration (a), MLD vs. chlorophyll concentration (b), MLD-averaged irradiance vs. carbon concentration (c), and MLD-averaged irradiance vs. chlorophyll concentration (d). Correlations are calculated at each grid cell using the 20-year satellite time series record.

526

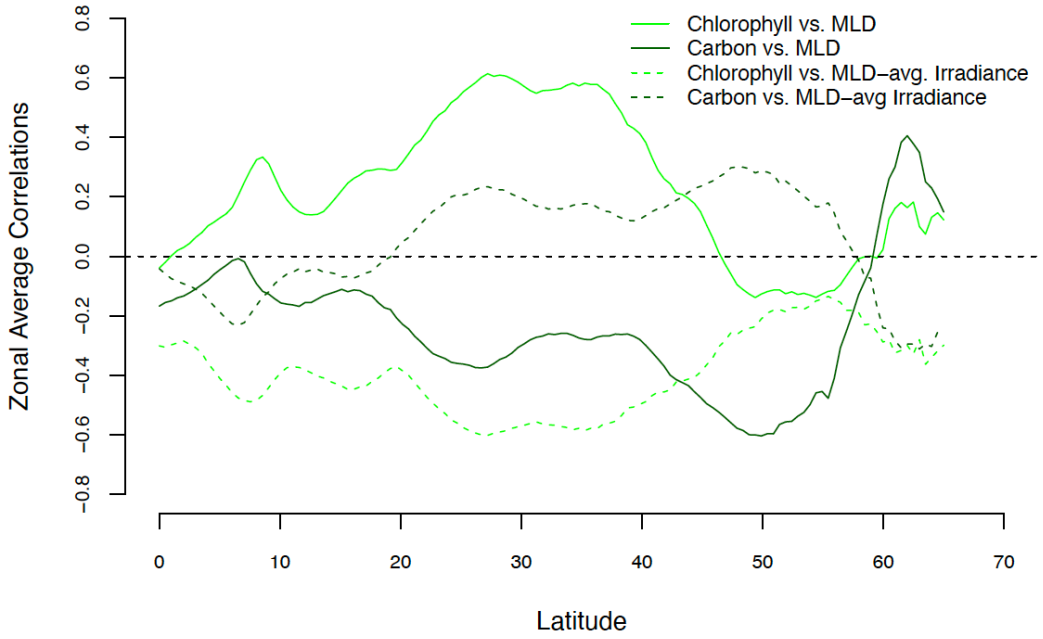

527

528 **Figure 7. Zonally averaged correlations of the maps presented in Figure 6.** Chlorophyll vs.
529 mixed layer depth (MLD) and chlorophyll vs. MLD-averaged irradiance are given in solid and
530 dashed light green lines, respectively. Carbon vs. mixed layer depth (MLD) and carbon vs.
531 MLD-averaged irradiance are given in solid and dashed dark green lines, respectively. Black
532 horizontal dashed line gives the zero-correlation line.

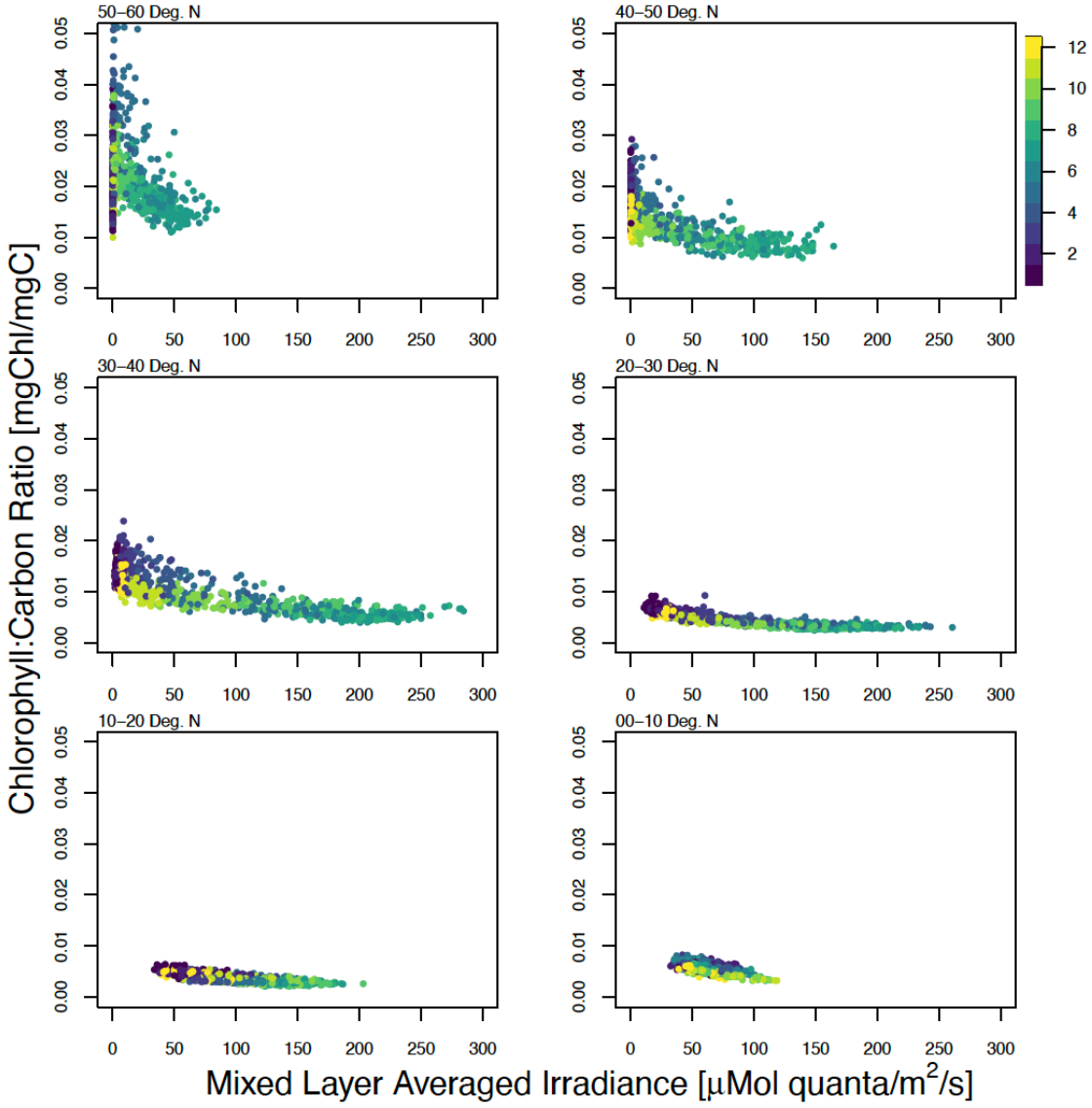

Figure 8. **Relationships between mixed layer-averaged irradiance and the satellite-estimated chlorophyll:carbon ratio.** Each box represents a ten-degree latitude band with the limits given in the upper left of each panel. Color represents month.

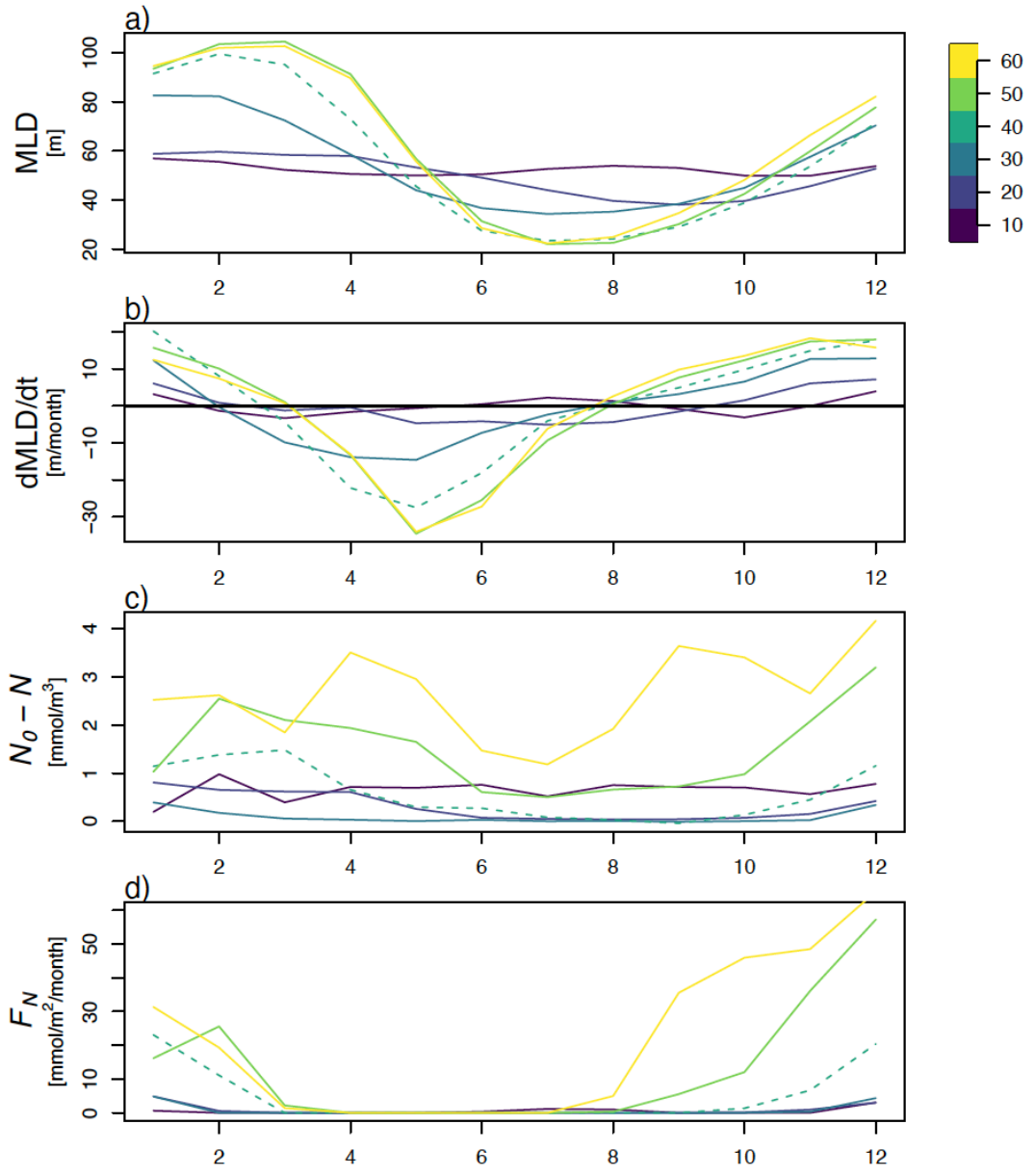

Figure 9. Climatological seasonal nitrate entrainment flux across latitudes. Colors represent ten-degree latitude bands as in Figure 5. Panel a gives the climatological seasonal cycle in mixed layer depth. Panel b gives the entrainment velocity (solid black gives the zero line). Panel c gives the nitrate gradient evaluated between the mixed layer and one meter below. Panel d gives the calculated entrainment flux. Dashed lines represent the transition zone (30-40°N).